<center>SUPPORTING INFORMATION</center>

Computational Screening of M_1/$PW_{12}O_{40}$ Single-Atom Electrocatalysts for Water Splitting and Oxygen Reduction Reactions

Shamraiz Hussain Talib[a,b], Babar Ali[c], Sharmarke Mohamed[a,b]*, Xue-Lian Jiang[d], Khalil Ahmad[e], Ahsanulhaq Qurashi[a,b]*, and Jun Li[d,f]*

[a]Advanced Materials Chemistry Centre (AMCC), Khalifa University of Science and Technology, Abu Dhabi, P.O. Box 127788, United Arab Emirates

[b]Department of Chemistry, Khalifa University of Science and Technology, Abu Dhabi, P.O. Box 127788, United Arab Emirates

[d]Department of Chemistry and Guangdong Provincial Key Laboratory of Catalytic Chemistry, Southern University of Science and Technology, Shenzhen 518055, China;

[c]King Fahd University of Petroleum and Minerals, School of Chemical and Materials Center for Refining and Advanced Chemicals (CRAC) at the Research and Innovation

[e]Department of Chemistry, Mirpur University of Science and Technology (MUST), Mirpur 10250, AJK, Pakistan

[f]Department of Chemistry and Engineering Research Center of Advanced Rare-Earth Materials of Ministry of Education, Tsinghua University, Beijing 100084, China;

Additional Computational Details

A cubic unit cell with a vacuum space of 20 Å contains a phosphotungstic acid (PTA) molecule with transition metal adatoms anchored at the four-fold hollow (4H) site. All the geometry optimization and energy calculation were performed using spin-polarized density functional theory (DFT) methods using the Vienna Ab Initio Simulation Package (VASP).[1-2] To improve the calculation efficiency, the projector augmented wave (PAW) pseudo-potentials are used to define the interaction between the valence and core electrons.[3-4] In this work, the generalized gradient approximation (GGA) using the Perdew, Burke, and Ernzerhof (PBE) exchange-correlation functional was adopted.[5-6] The Kohn-Sham orbitals are expanded by using plane-wave basis sets with an energy cutoff of 400 eV. The geometry optimization was done with a convergence criterion of 10^{-5} eV for the total energy. All the ions are permitted to relax until the maximum force is less than 0.02 eV/Å. The Brillion zone integration was sampled using a 1 x 1 x 1 Γ point. A k-point mesh of $3\times3\times3$ was tested for sampling the Brillouin zone and no significant difference was found between the 1 x 1 x 1 Γ point sampling.

The Bader charge analysis was performed to compute the electron charge transfer.[7-9] To model the PTA cluster we first constructed a periodic supercell containing 4 x 4 primitive cells (with 12 W atoms, one P atom, and 40 O atoms). By using the standard hydrogen electrode (SHE), the Gibbs free energy change (ΔG) of every elemental step was calculated.

Under standard conditions, HER catalytic property was defined by using the free energy difference of hydrogen adsorption (ΔG_H), which was attained by computing the following equation:

$$\Delta G_H = \Delta E_H + \Delta E_{ZPE} - T\Delta S_H \tag{1}$$

Where ΔE_H is the hydrogen adsorption energy, ΔE_{ZPE} is the difference between the zero-point energies of the adsorbed hydrogen and gas phase hydrogen, and ΔS_H is the entropy difference between the gas phase and adsorbed state. The pressure is 1 atom and temperature $T = 298$ K. Furthermore, the ΔE_{ZPE} and $T\Delta S_H$ values can be calculated through the vibrational frequencies of the system.

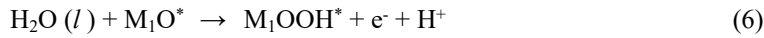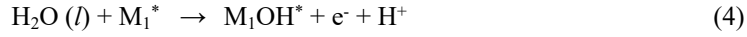ΔE_H is defined as the following using the computational hydrogen electrode (CHE) model:

$$\Delta E_H = E_{(catalyst + H)} - E \text{ (catalyst)} - 1/2 \, E_{H2} \tag{2}$$

Where $E_{(catalyst + H)}$ is the calculated adsorption energies of the M_1/PTA system with adsorption of one H atom, and E (catalyst) represents the energies of the M_1/PTA system without adsorption of H. The ideal value of ΔE_H is zero, signifying that the better HER performance.

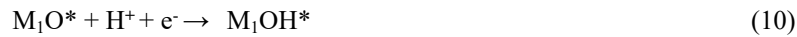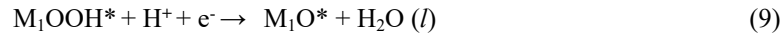When the pH was fixed to zero, the overall OER could be defined as follows.[10-11]

$$2H_2O \rightarrow 4H^+ + O_2 + 4e^- \tag{3}$$

The following are the four-electron reaction steps for OER processes:

$$H_2O \, (l) + M_1^* \rightarrow M_1OH^* + e^- + H^+ \tag{4}$$

$$M_1OH^* \rightarrow M_1O^* + e^- + H^+ \tag{5}$$

$$H_2O \, (l) + M_1O^* \rightarrow M_1OOH^* + e^- + H^+ \tag{6}$$

$$M_1OOH^* \rightarrow O_2 \, (g) + e^- + H^+ + M_1^* \tag{7}$$

Where M_1^* refers to the catalyst and active adsorption site on the catalyst; (l) and (g) represent the liquid and gas phases, respectively; and OH^*, $O^{*,}$ and OOH^* represent the corresponding adsorbed intermediates.

The ORR processes can be observed as the opposite of OER,[12] and the four key adsorption/desorption steps are written as below:

$$M_1^* + O_2 \, (g) + H^+ + e^- \rightarrow M_1OOH^* \tag{8}$$

$$M_1OOH^* + H^+ + e^- \rightarrow M_1O^* + H_2O \, (l) \tag{9}$$

$$M_1O^* + H^+ + e^- \rightarrow M_1OH^* \tag{10}$$

$$M_1OH^* + H^+ + e^- \rightarrow M_1^* + H_2O \tag{11}$$

The Gibbs free energy difference for all the above elementary steps (ΔG_{OH*}, ΔG_{O*}, ΔG_{OOH*}) comprises an electron transfer that would be calculated by using the following equations:

$$\Delta G = \Delta E + \Delta ZPE - T\Delta S + \Delta G_U + \Delta G_{pH} \tag{12}$$

Where ΔE, ΔZPE, and ΔS are the energy difference of adsorption energy, zero-point energy, and entropy, respectively.[13] The adsorption energies of ΔE are calculated by using DFT. The ΔZPE and $T\Delta S$ were calculated by

using DFT and the standard thermodynamic data. $\Delta G_U = -eU$, is the free energy change related to the electrode-potential U. $\Delta G_{pH} = -kT \ln 10^* pH$, with ΔG_{PH} denoting the Gibbs free energy which is amended by H^+ concentration.

The Gibbs free energy changes of four elementary steps for OER processes can be defined as: $\Delta G_a = \Delta G_{OH^*}$, $\Delta G_b = \Delta G_{O^*} - \Delta G_{OH^*}$, $\Delta G_c = \Delta G_{OOH^*} - \Delta G_{O^*}$, $\Delta G_d = 4.92 - \Delta G_{OOH^*}$. For ORR steps: $\Delta G_1 = \Delta G_{OOH^*} - 4.92$, $\Delta G_2 = \Delta G_{O^*} - \Delta G_{OOH^*}$, $\Delta G_3 = \Delta G_{OH^*} - \Delta G_{O^*}$, $\Delta G_4 = \Delta G_{OH^*}$.

Under electrode potential U = 0 V, the ΔG for all the four elementary steps can be calculated by:

i) $\Delta G_a = G(HO^*) + G(H^+ + e^-) - G(H_2O) - G(*)$

Or $\Delta G_a = G(HO^*) + 1/2G(H_2) - G(H_2O) - G(*)$

$= (E_{OH^*} + ZPE_{OH^*} - TS_{OH^*}) + 1/2(E_{H2} + ZPE_{H2} - TS_{H2}) - (E_{H2O} + ZPE_{H2O} - TS_{H2O}) - E^*$

ii) $\Delta G_b = G(O^*) + G(H^+ + e^-) - G(OH^*)$

Or $\Delta G_b = G(O^*) + G(H_2) - G(OH^*)$

$= (E_{O^*} + ZPE_{O^*} - TS_{O^*}) + 1/2(E_{H2} + ZPE_{H2} - TS_{H2}) - (E_{OH^*} + ZPE_{OH^*} - TS_{OH^*})$

iii) $\Delta G_c = G(HOO^*) + G(H^+ + e^-) - G(H_2O) - G(O^*)$

Or $\Delta G_c = G(HOO^*) + 1/2G(H_2) - G(H_2O) - G(O^*)$

$= (E_{OOH^*} + ZPE_{OOH^*} - TS_{OOH^*}) + 1/2(E_{H2} + ZPE_{H2} - TS_{H2}) - (E_{O^*} + ZPE_{O^*} - TS_{O^*})$

iv) $\Delta G_d = G(O_2) + G(H^+ + e^-) - G(OOH^*)$

Or $\Delta G_d = \{4.92 + 2G(H_2O) - 2G(H_2)\} + 1/2G(H_2) - G(OOH^*)$

$= \{4.92 + E_{H2O} + ZPE_{H2O} - TS_{H2O}) - 2(E_{H2} + ZPE_{H2} - TS_{H2})\} + 1/2(E_{H2} + ZPE_{H2} - TS_{H2}) - (E_{OOH^*} + ZPE_{OOH^*} - TS_{OOH^*})$

Or $= 4.92 + 2(E_{H2O} + ZPE_{H2O} - TS_{H2O}) - 3/2(E_{H2} + ZPE_{H2} - TS_{H2}) - (E_{OOH^*} + ZPE_{OOH^*} - TS_{OOH^*})$

where the asterisk (*) refers to the catalyst and active adsorption site on the catalyst. Moreover, the error arising from the computing of the triplet O_2 molecule with DFT methods can be corrected by fixing the overall Gibbs reaction energy, with Gibbs free energy of O_2 to the experimental value of 4.92 eV. Hence, an ideal catalyst with overpotential (η) = 0 V would perfectly allocate the overall change in Gibbs free energy throughout the four elementary OER/ORR steps i.e., $\Delta G_{a-d} = 1.23$ eV.

If the ΔG value of all the four elementary steps is different, the overpotential (η) used to further rationalize the catalytic performance of OER and ORR would be calculated by using the following equations:

$$\eta^{OER} = \max \{\Delta G_a, \Delta G_b, \Delta G_c, \Delta G_d\} / e - 1.23 \qquad (13)$$

$$\eta^{ORR} = \max \{\Delta G_1, \Delta G_2, \Delta G_3, \Delta G_4\} / e + 1.23 \qquad (14)$$

Volcano Curve

In the volcano curve, the Gibbs free energies of hydrogen adsorption (ΔG_{H*}) over the PTA cluster with a hydrogen coverage of $\theta = 1$ and PTA cluster with a hydrogen coverage of $\theta = 1/2$ are used to calculate the exchange current, (i_0). To obtain ΔG_{H*}, the equation S2 was rewritten to:

$$\Delta E_H = E_{nH*} - E_{cat} - \frac{n}{2} E_{H_2} \qquad (S15)$$

where the asterisk denotes the catalyst. E_{nH*}, $E_{(n-1)\,H*}$, and E_{H2} represent the total energies of the catalyst with n adsorbed hydrogen atoms, the catalyst with $n-1$ adsorbed atomic hydrogen, and the H_2 gas, respectively. The i_0 value is evaluated based on Norskov's theory (see the reference for details). If $\Delta G_{H*} \leq 0$, the following equation is used to calculate the exchange current at pH= 0:

$$i_0 = -ek_0 \frac{1}{1 + \exp\left(-\Delta G_{H*}/k_b T\right)} \qquad (S16)$$

For another case if the $\Delta G_{H*} > 0$, the i_0 is calculated by using the following expression at pH= 0:

$$i_0 = -ek_0 \frac{1}{1 + \exp\left(\Delta G_{H*}/k_b T\right)} \qquad (S17)$$

where k_0 is the rate constant. As there are no experimental data available, k_0 is set to 1. k_B is the Boltzmann constant ($k_B = 1.380\,649 \times 10^{-23}$ J K^{-1}) and T is the temperature (T=298.15 K).

d-band Center

The value of the d-band center of the embedded single metal atoms over the PTA cluster can be calculated by using the following equation:

$$\varepsilon d = \frac{\int_{-\infty}^{\infty} n_d(\varepsilon)\varepsilon d\varepsilon}{\int_{-\infty}^{\infty} n_d(\varepsilon)d\varepsilon} \qquad (S18)$$

Where the n_d denotes the d states of the single metal atoms (M_1) embedded in the PTA cluster. The d-band center of the M_1 atoms, which are closely associated with the catalytic activity and can be calculated by the above-mentioned equation.
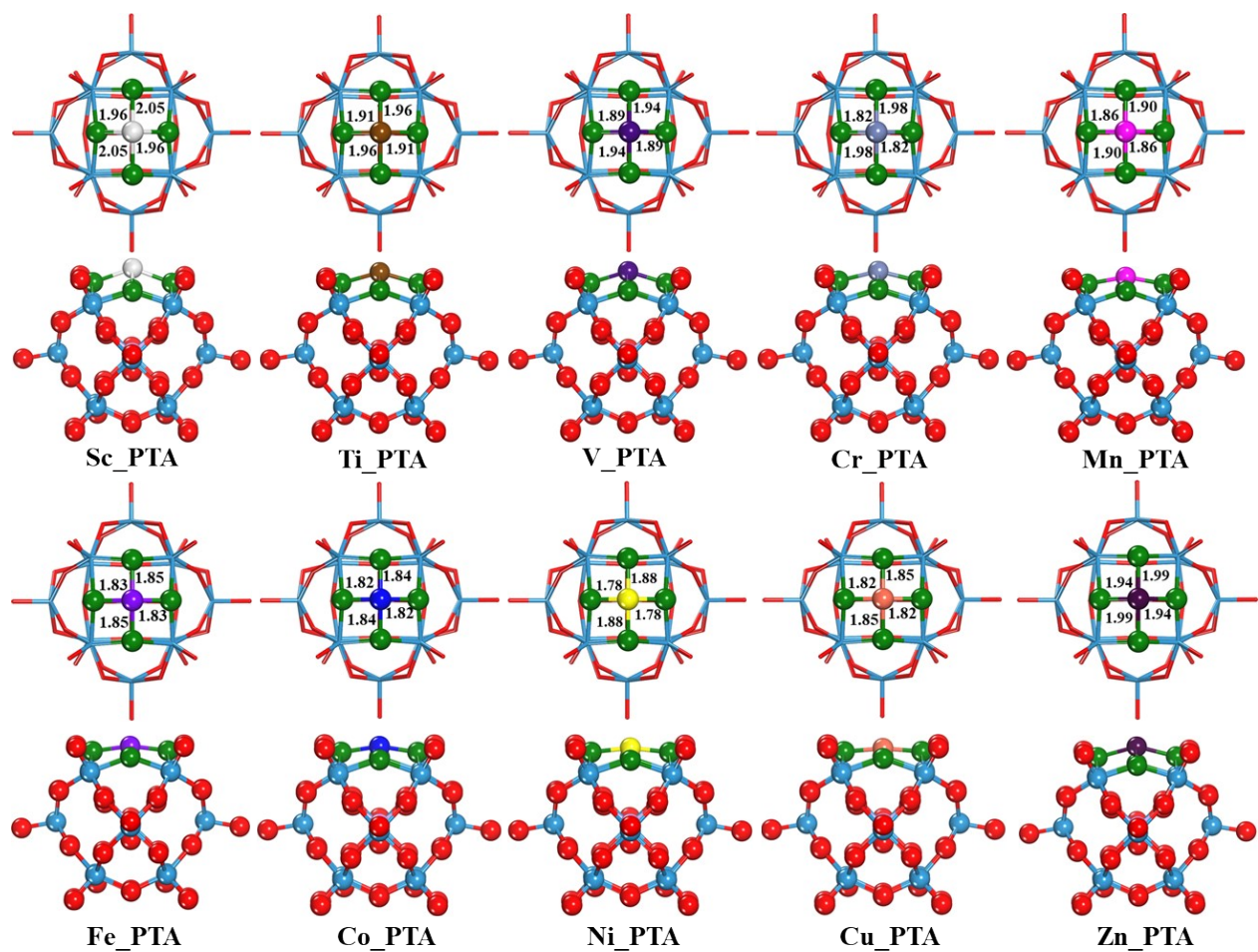
Fig. S1. Top and side views of the optimized configuration of 3d transition metal atoms (Sc_1, Ti_1, V_1, Cr_1, Mn_1, Fe_1, Co_1, Ni_1, Cu_1, and Zn_1) attached on the PTA support. All the bond lengths are given in Å.
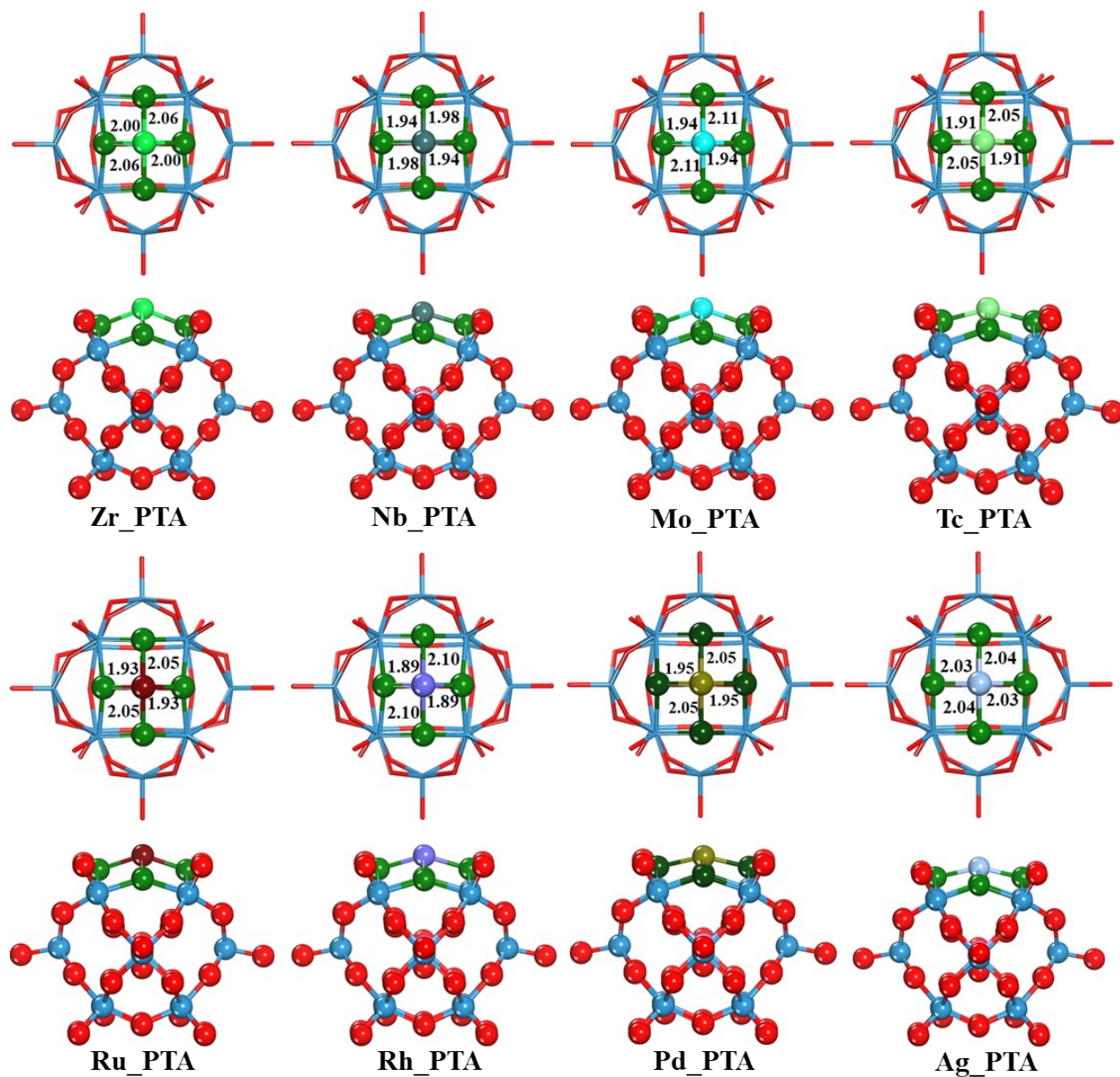
Fig. S2. Top and side views of the optimized configuration of 4d transition metal atoms (Zr_1, Nb_1, Mo_1, Tc_1, Ru_1, Rh_1, Pd_1, and Ag_1) attached on the PTA support. All the bond lengths are given in Å.
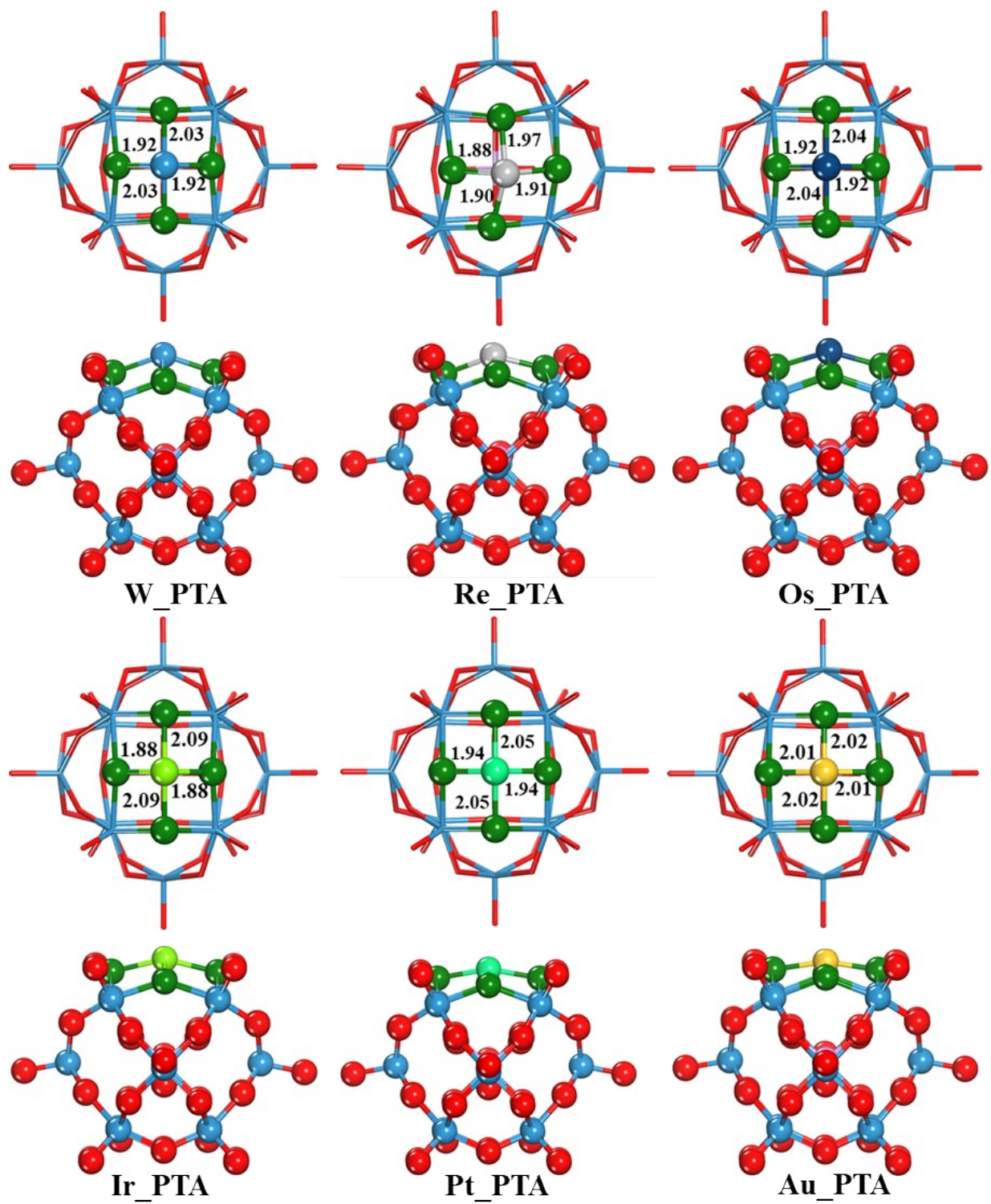
Fig S3. Top and side views of the optimized configuration of 5d transition metal atoms (W_1, Re_1, Os_1, Ir_1, Pt_1, and Au_1) attached to the PTA support. All the bond lengths are given in Å.

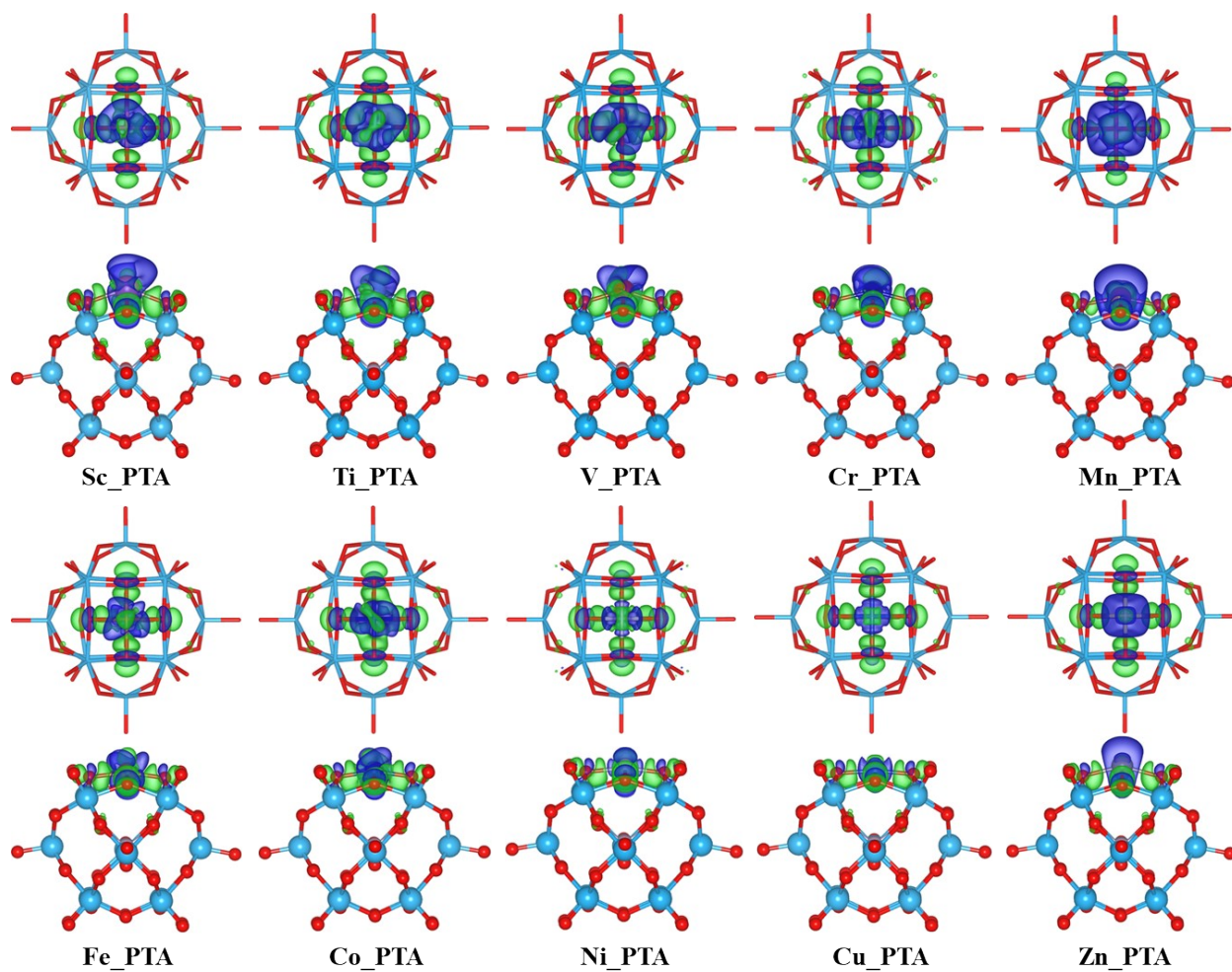**Fig S4.** Top and side view of partial electron density differences (PEDD) of 3d transition metal atoms (Sc_1, Ti_1, V_1, Cr_1, Mn_1, Fe_1, Co_1, Ni_1, Cu_1, and Zn_1) attached on the PTA support. For the contour plots, the charge accumulation regions are rendered in Green while the charge depletion regions are shown in blue. The contour value of the electron difference density is ±0.005 a.u.
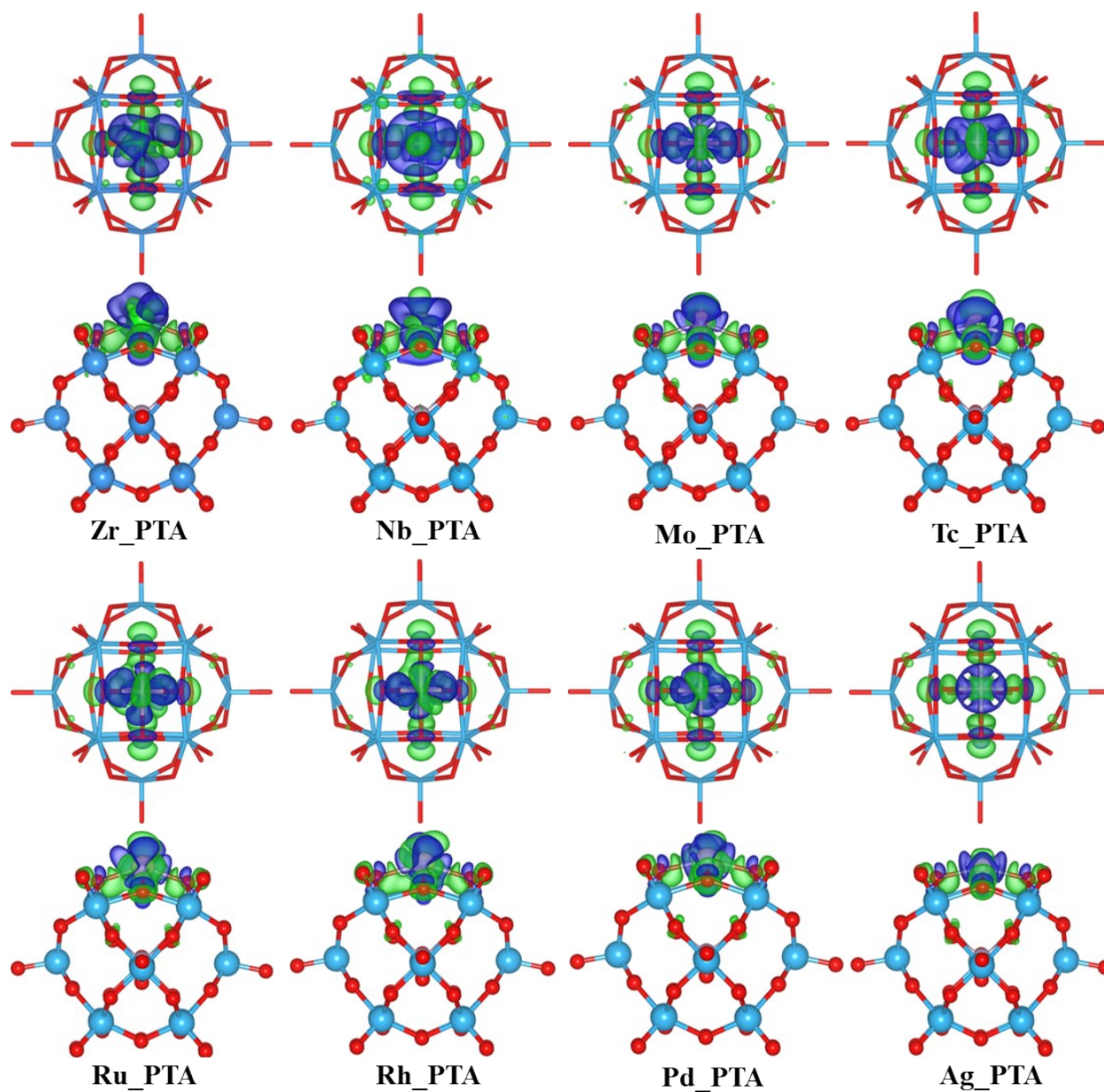
Fig S5. Top and side view of partial electron density differences (PEDD) of 4d transition metal atoms (Zr_1, Nb_1, Mo_1, Tc_1, Ru_1, Rh_1, Pd_1, and Ag_1) attached on the PTA support. For the contour plots, the charge accumulation regions are rendered in green while the charge depletion regions are shown in blue. The contour value of the electron difference density is ±0.005 a.u.
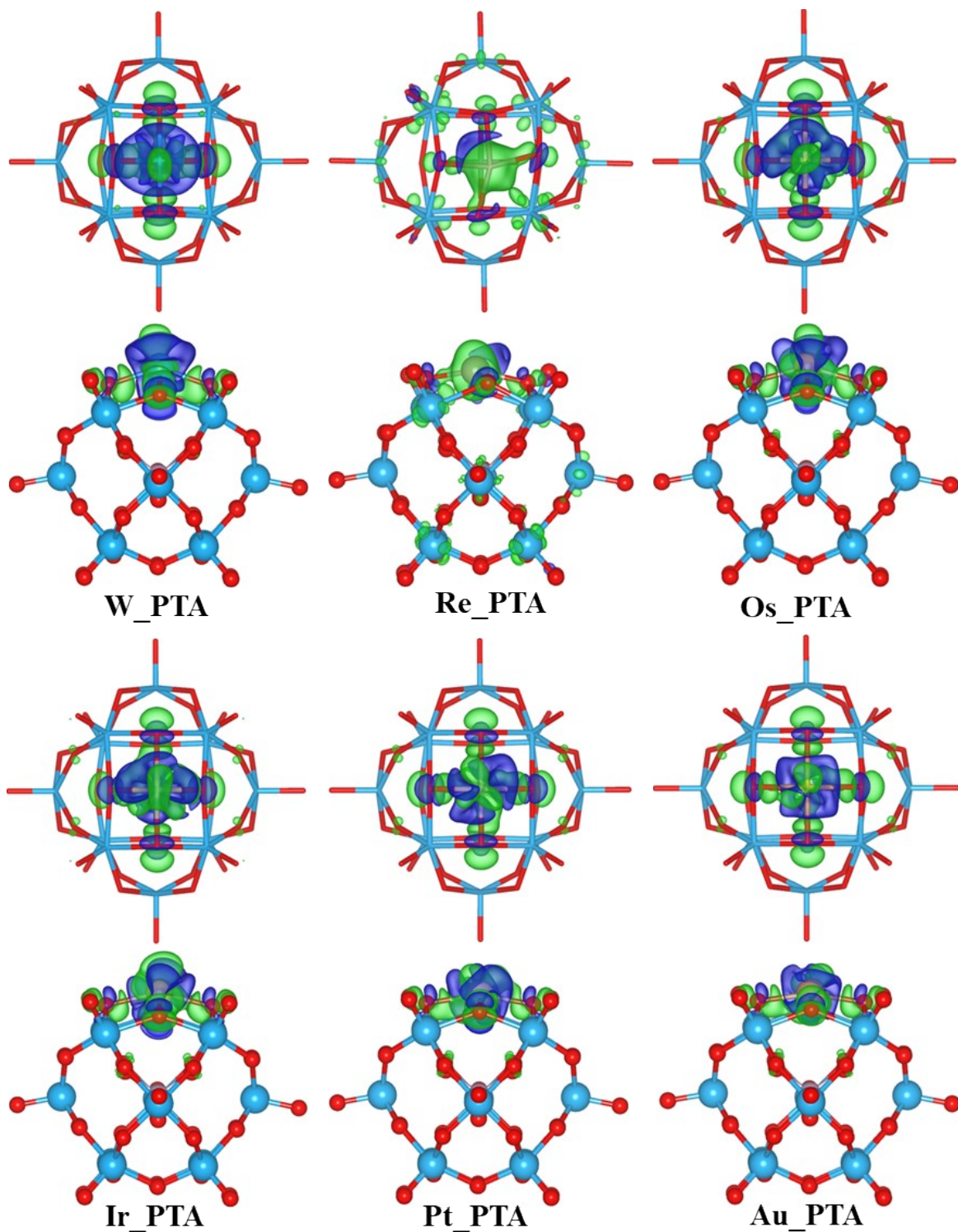
Fig. S6. Top and side view of partial electron density differences (PEDD) of 5d transition metal atoms (W_1, Re_1, Os_1, Ir_1, Pt_1, and Au_1) attached on the PTA support. For the contour plots, the charge accumulation regions are rendered in green while the charge depletion regions are shown in blue. The contour value of the electron difference density is ±0.005 a.u.
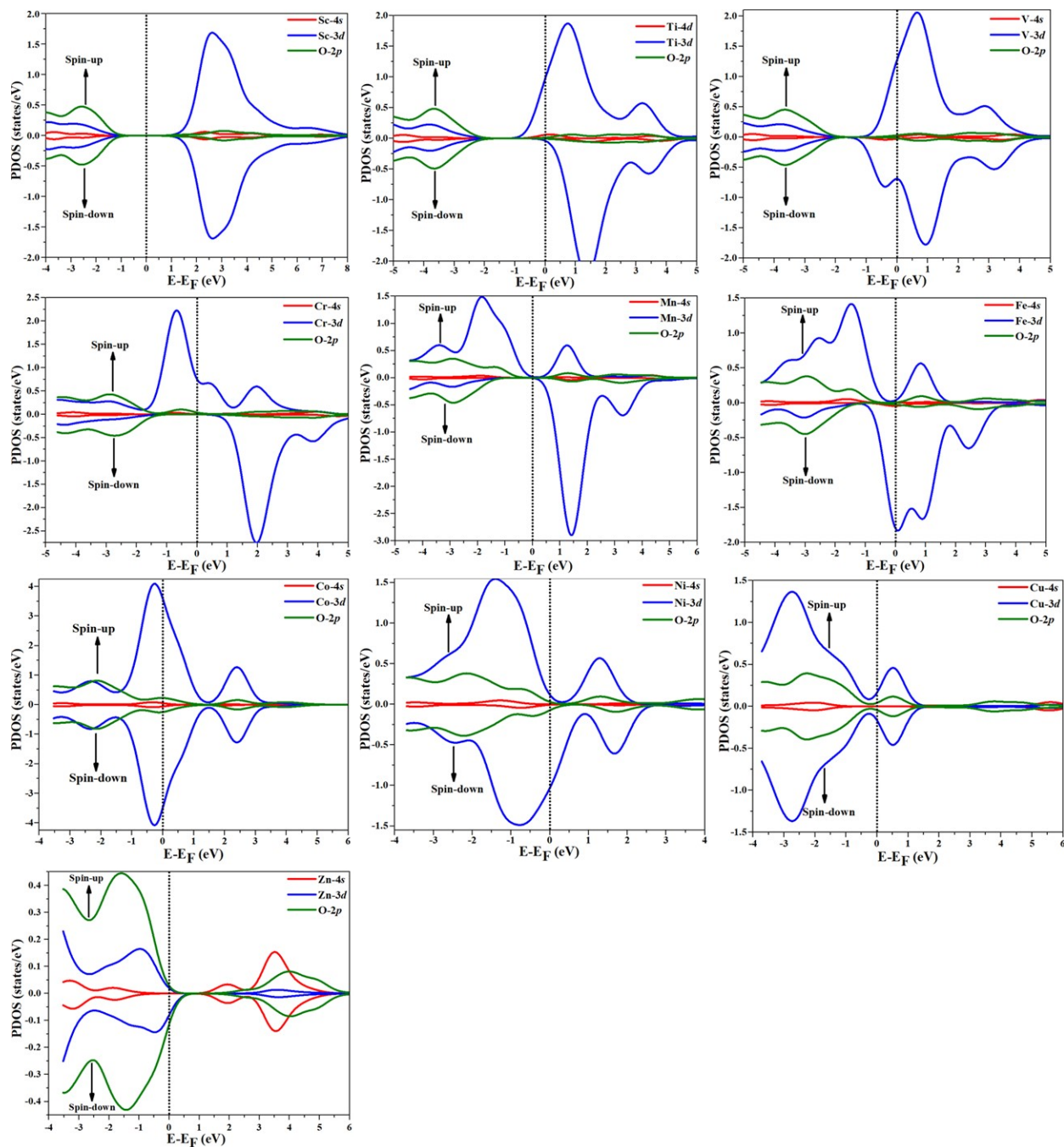
Fig. S7. The spin-polarized partial density of states (PDOS) of 3d transition metal atoms (Sc$_1$, Ti$_1$, V$_1$, Cr$_1$, Mn$_1$, Fe$_1$, Co$_1$, Ni$_1$, Cu$_1$, and Zn$_1$) attached to the PTA support. PDOS projected on M$_1$-3d (blue) and M$_1$-4s (red) and O-2p (olive) states. The Fermi level is fixed at zero.

Fig. S8. The spin-polarized partial density of states (PDOS) of 4d transition metal atoms (Zr$_1$, Nb$_1$, Mo$_1$, Tc$_1$, Ru$_1$, Rh$_1$, Pd$_1$, and Ag$_1$) attached to the PTA support. PDOS projected on M$_1$-4d (blue) and M$_1$-5s (red) and O-2p (olive) states. The Fermi level is fixed at zero.
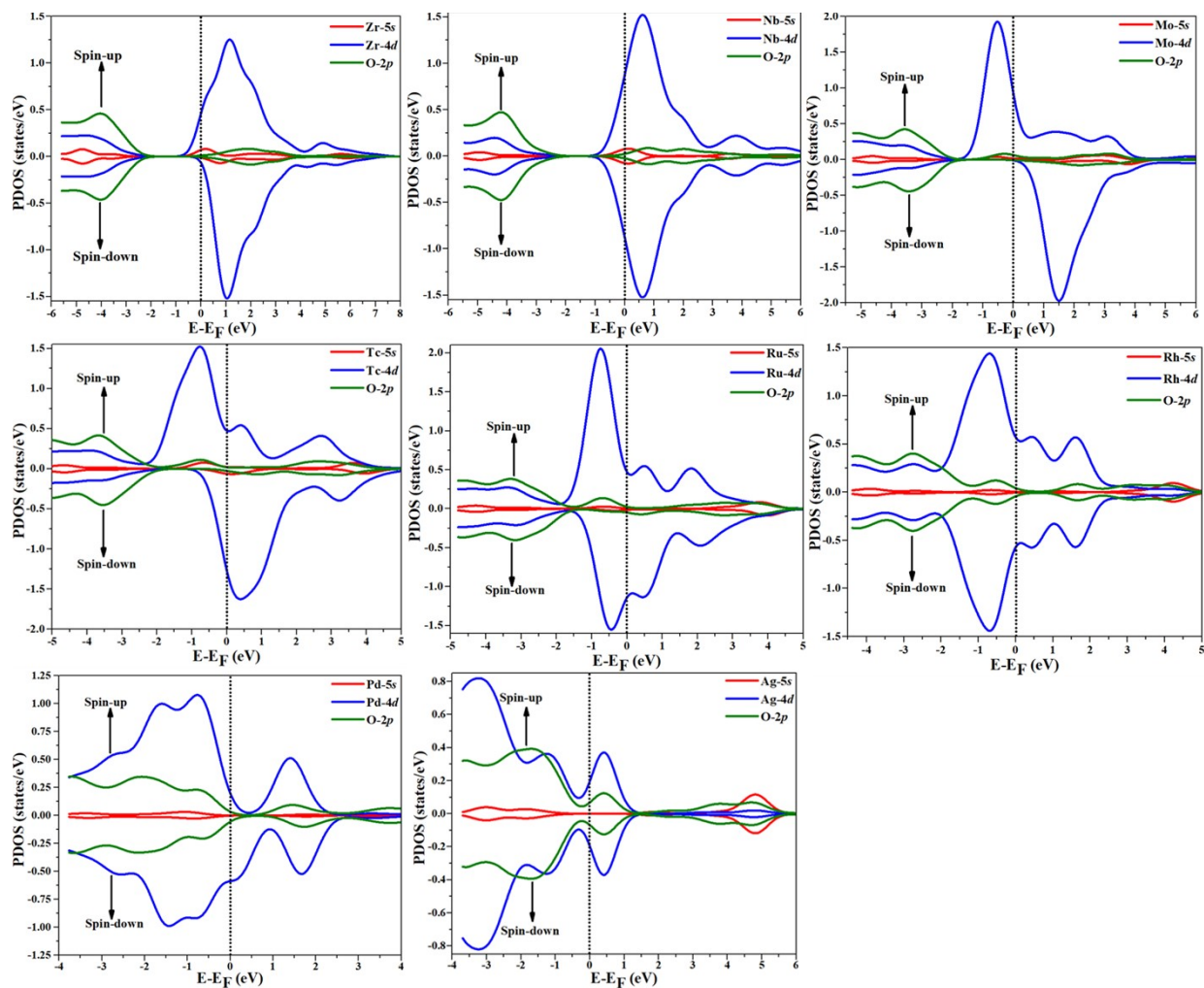
Fig. S9. The spin-polarized partial density of states (PDOS) of 5d transition metal atoms (W_1, Re_1, Os_1, Ir_1, Pt_1, and Au_1) attached to the PTA support. PDOS projected on M_1-5d (blue) and M_1-6s (red) and O-2p (olive) states. The Fermi level is fixed at zero.
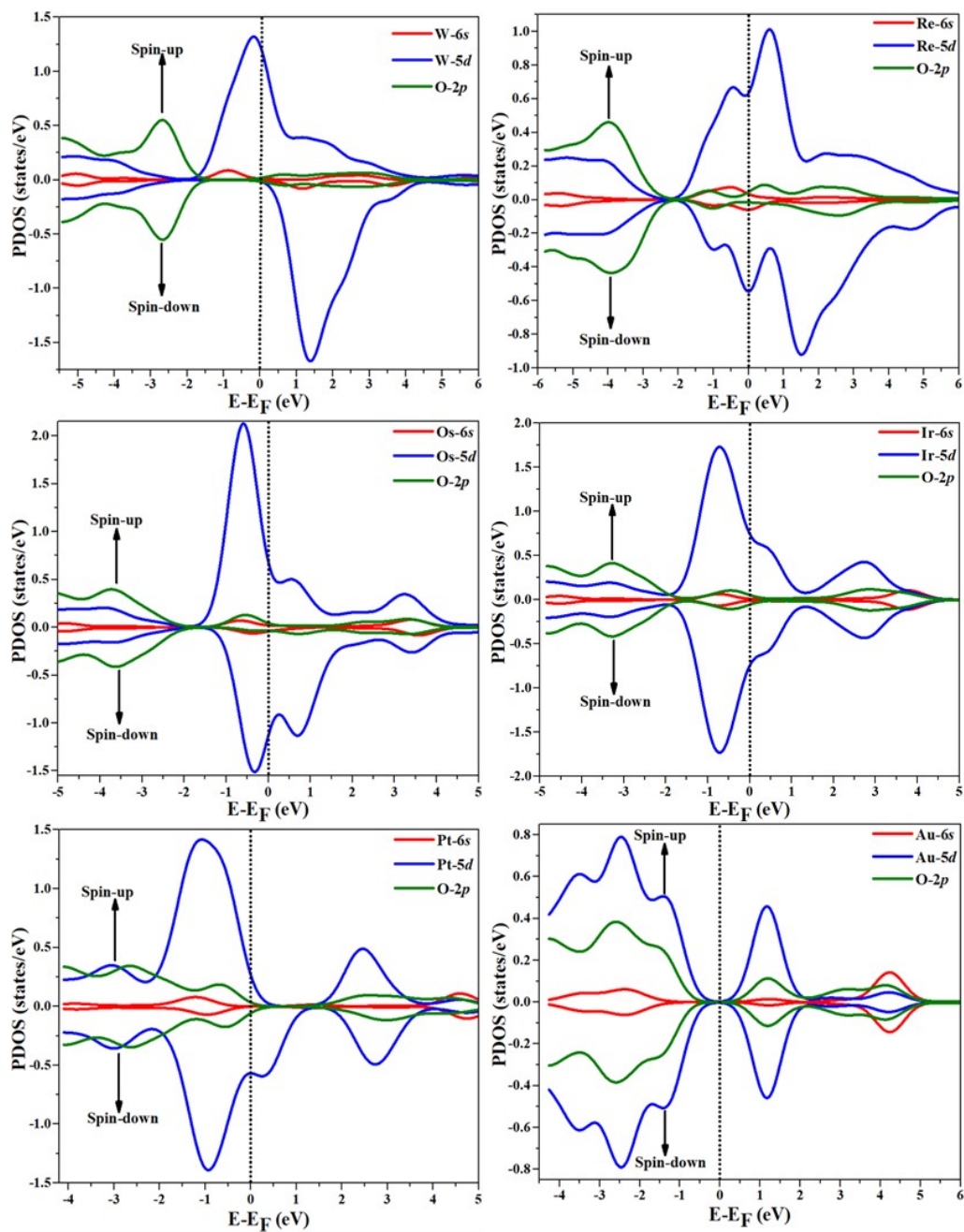
Table S1. The binding sites, calculated binding energies (eV), average bond lengths between the metal atoms and neighboring oxygen atoms (Å), and Bader charges [$q(e^-)$] of transition metal atoms (3d = Sc_1, Ti_1, V_1, Cr_1, Mn_1, Fe_1, Co_1, Ni_1, Cu_1, Zn_1: 4d = Zr_1, Nb_1, Mo_1, Tc_1, Ru_1, Rh_1, Pd_1, Ag_1: 5d = W_1, Re_1, Os_1, Ir_1, Pt_1, Au_1) anchored on the PTA support.

| Systems	Binding Site	E_{bin}/eV	Average Bond Length (Å)	q (e)
Sc_1/PTA	4H-site	-10.54	2.01	1.79
Ti_1/PTA	4H-site	-8.45	1.94	1.64
V_1/PTA	4H-site	-7.17	1.92	1.50
Cr_1/PTA	4H-site	-6.69	1.90	1.47
Mn_1/PTA	4H-site	-6.41	1.88	1.39
Fe_1/PTA	4H-site	-5.13	1.84	0.84
Co_1/PTA	4H-site	-4.36	1.83	0.88
Ni_1/PTA	4H-site	-3.99	1.83	0.92
Cu_1/PTA	4H-site	-3.37	1.84	0.79
Zn_1/PTA	4H-site	-4.11	1.97	0.90
Zr_1/PTA	4H-site	-8.59	2.03	2.05
Nb_1/PTA	4H-site	-5.78	1.96	1.89
Mo_1/PTA	4H-site	-4.70	2.03	1.77
Tc_1/PTA	4H-site	-3.19	1.98	1.54
Ru_1/PTA	4H-site	-2.50	1.99	1.49
Rh_1/PTA	4H-site	-2.45	2.00	0.95
Pd_1/PTA	4H-site	-2.09	2.00	1.06
Ag_1/PTA	4H-site	-1.59	2.04	0.74
W_1/PTA	4H-site	-3.80	1.98	3.49
Re_1/PTA	4H-site	-2.56	1.92	1.80
Os_1/PTA	4H-site	-1.31	1.98	1.23
Ir_1/PTA	4H-site	-1.44	1.98	0.52
Pt_1/PTA	4H-site	-1.67	1.99	0.61
Au_1/PTA	4H-site	-1.36	2.02	0.54
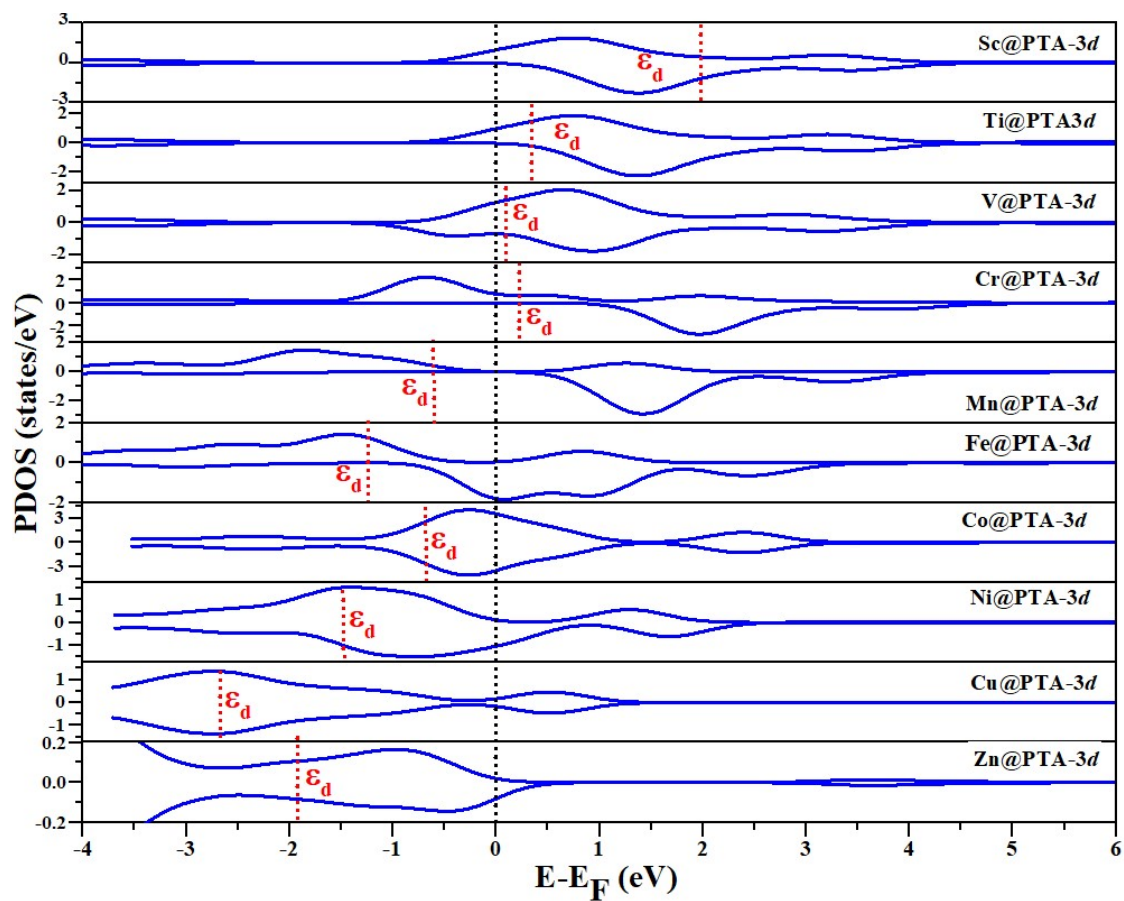
Fig. S10. Calculated spin-polarized partial density of states (PDOS) of the d-band of the 3d transition metal atoms (Sc_1, Ti_1, V_1, Cr_1, Mn_1, Fe_1, Co_1, Ni_1, Cu_1, and Zn_1) attached on the PTA support. PDOS proposed on M_1-3d (blue) states. The Fermi level is fixed at the zero of energy and the d-band center (ε_d) is marked by the red dashed line.
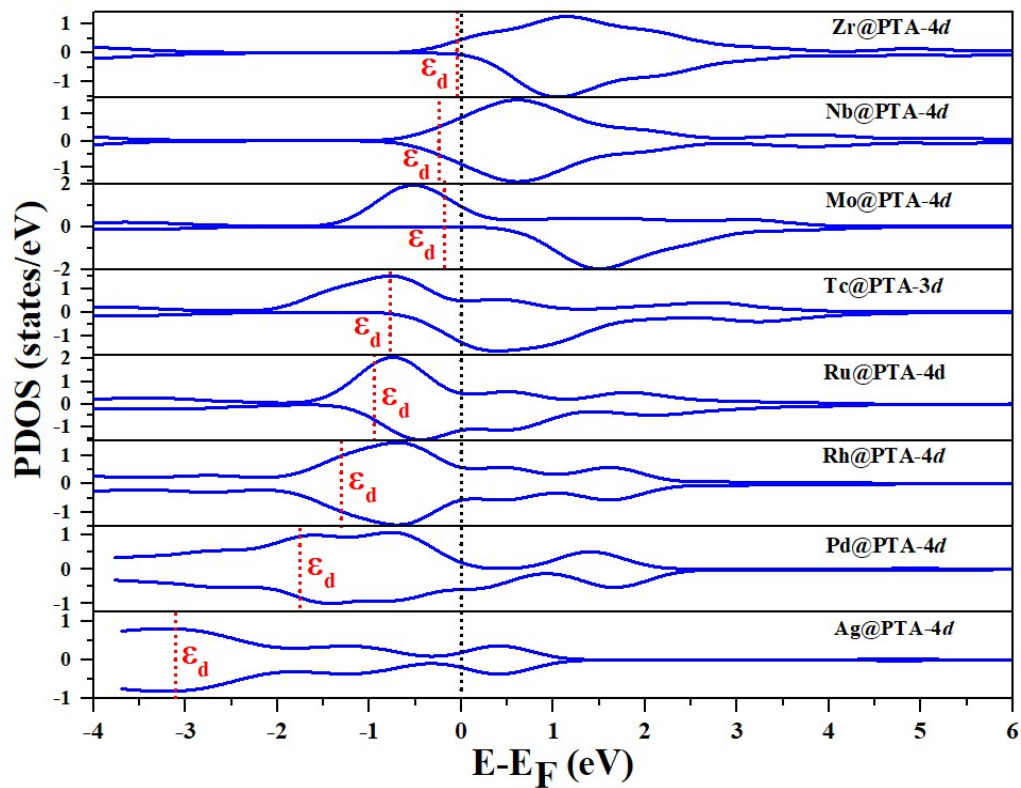
S15

Fig. S11. Calculated spin-polarized partial density of states (PDOS) of the d-band of the 4d transition metal atoms (Zr_1, Nb_1, Mo_1, Tc_1, Ru_1, Rh_1, Pd_1, and Ag_1) attached on the PTA support. PDOS projected on M_1-4d (blue) states. The Fermi level is fixed at the zero of energy and the d-band center (ε_d) is marked by the red dashed line.
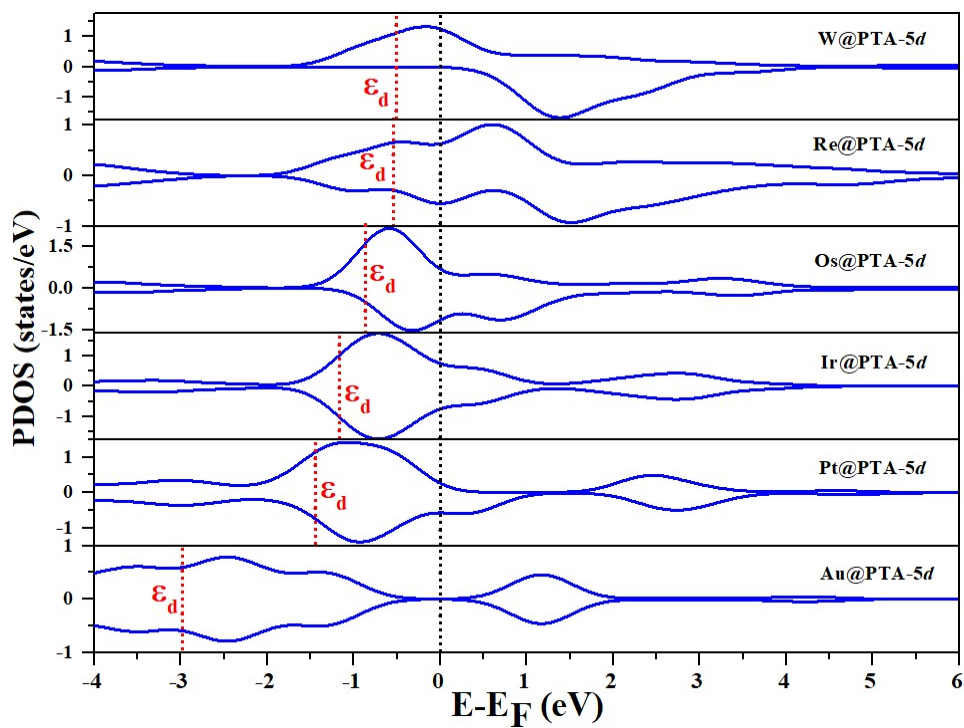
Fig. S12. Calculated spin-polarized partial density of states (PDOS) of the d-band of the 5d transition metal atoms (W_1, Re_1, Os_1, Ir_1, Pt_1, and Au_1) attached on the PTA support. PDOS proposed on M_1-5d (blue) states. The Fermi level is fixed at the zero of energy and the d-band center (ε_d) is marked by the red dashed line.
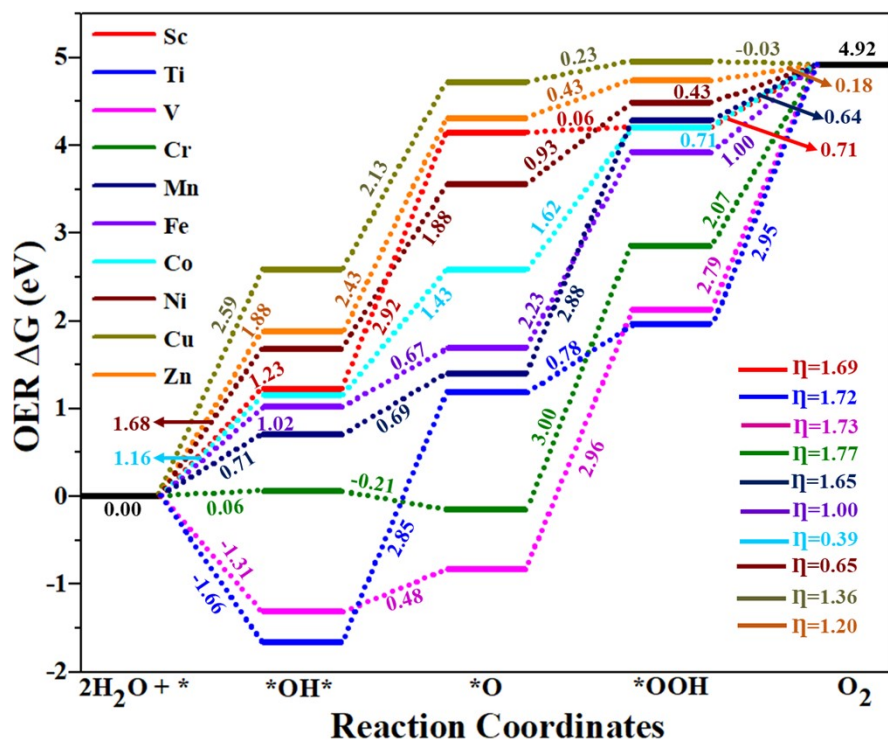
Fig. S13. Calculated free energy diagram for the OER over 3d M_1/PTA (M_1= Sc_1, Ti_1, V_1, Cr_1, Mn_1, Fe_1, Co_1, Ni_1, Cu_1, and Zn_1) cluster under U= 0 V and the corresponding changes of free energies and theoretical overpotential (η).
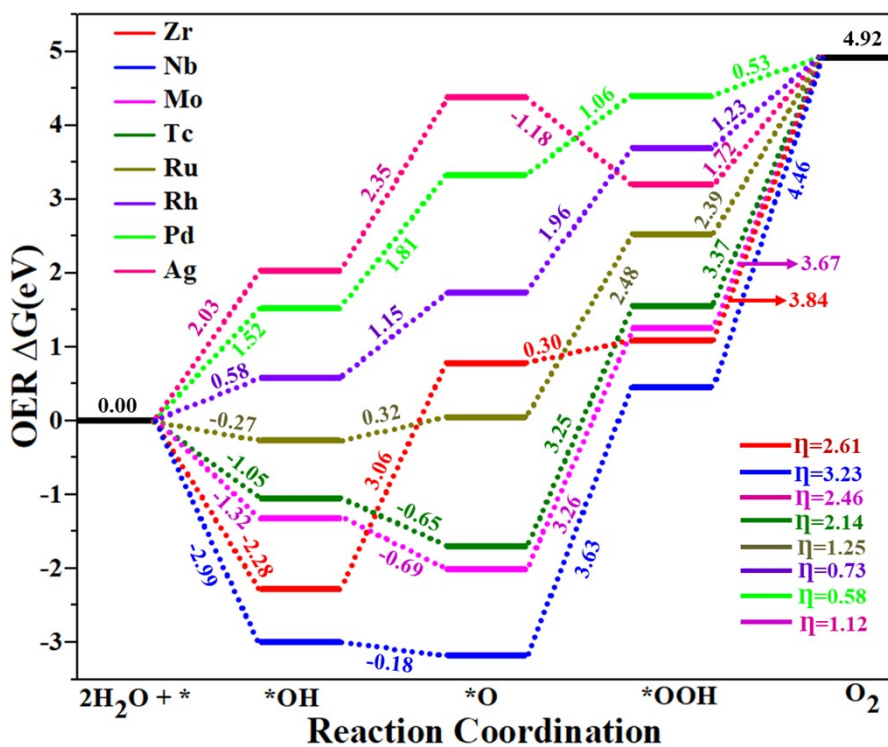
Fig. S14. Calculated free energy diagram for the OER over 4d M_1/PTA (Zr_1, Nb_1, Mo_1, Tc_1, Ru_1, Rh_1, Pd_1, and Ag_1) cluster under U= 0 V and the corresponding changes of free energies and theoretical overpotential (η).
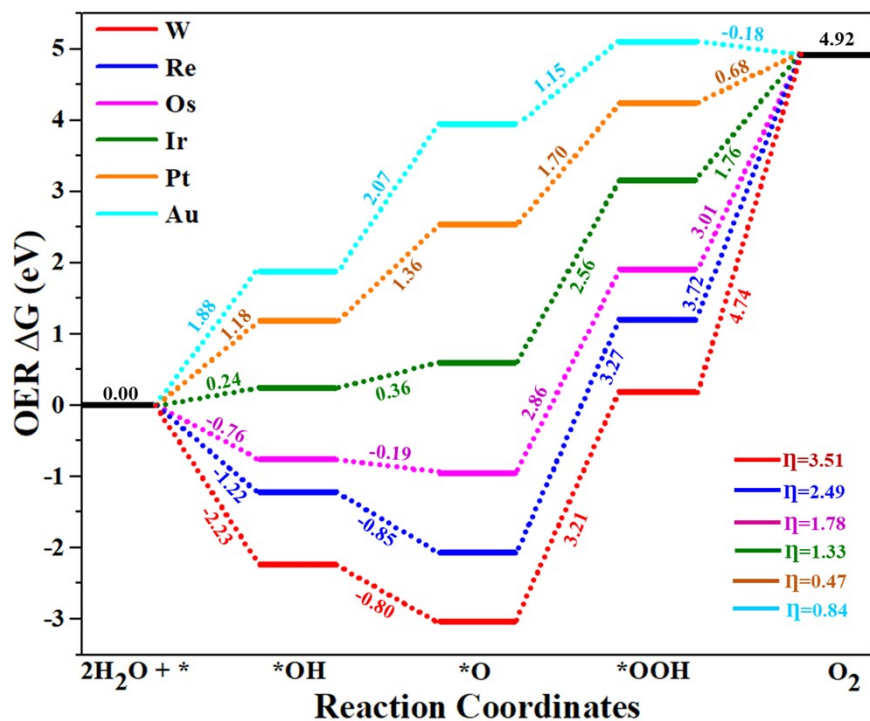
Fig. S15. Calculated free energy diagram for the OER over 5d M_1/PTA (M_1= W_1, Re_1, Os_1, Ir_1, Pt_1, and Au_1) cluster under U= 0 V and the corresponding changes of free energies and theoretical overpotential (η).
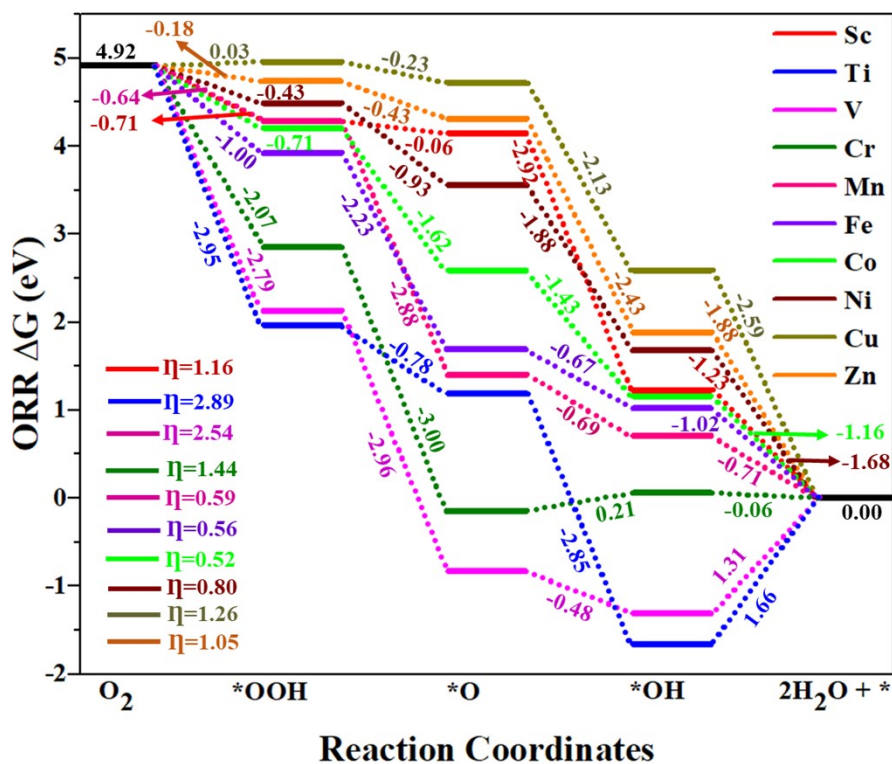
Fig. S16. Calculated free energy diagram for the ORR over 3d M_1/PTA (M_1= Sc_1, Ti_1, V_1, Cr_1, Mn_1, Fe_1, Co_1, Ni_1, Cu_1, and Zn_1) cluster under U= 0 V and the corresponding changes of free energies and theoretical overpotential (η).
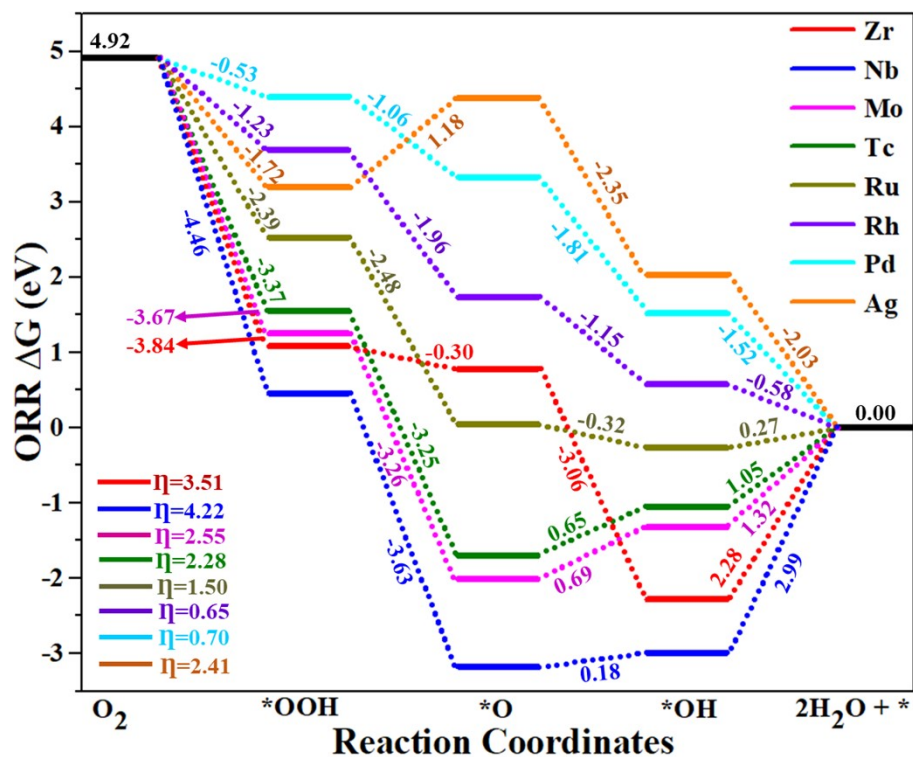
Fig. S17. Calculated free energy diagram for the ORR over 4d M_1/PTA (Zr_1, Nb_1, Mo_1, Tc_1, Ru_1, Rh_1, Pd_1, and Ag_1) support under U= 0 V and the corresponding changes of free energies and theoretical overpotential (η).
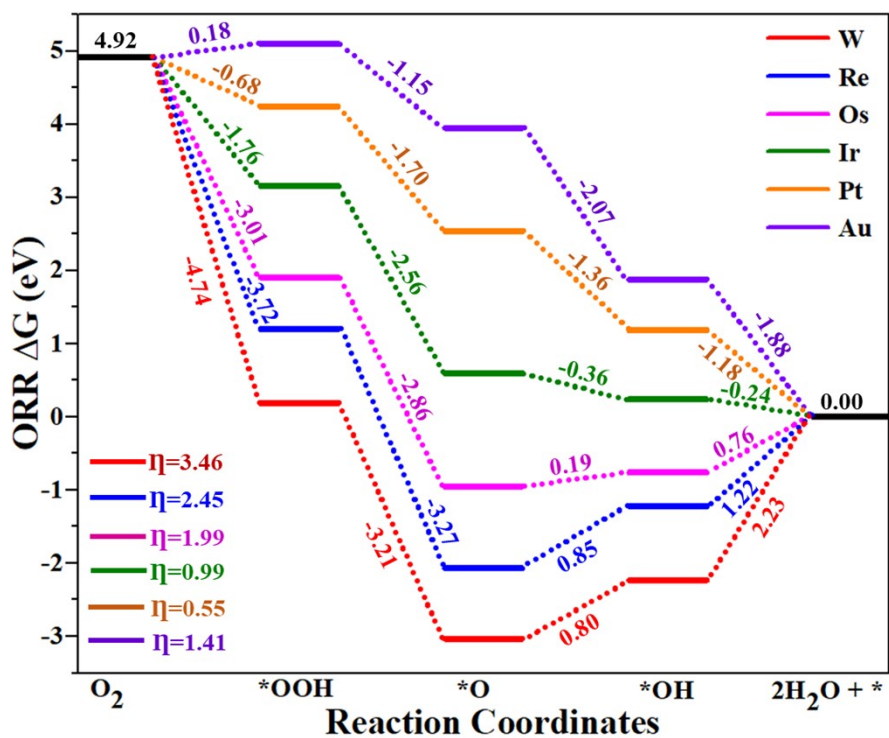
Fig. S18. Calculated free energy diagram for the ORR over 5d M_1/PTA (M_1= W_1, Re_1, Os_1, Ir_1, Pt_1, and Au_1) support under U= 0 V and the corresponding changes of free energies and theoretical overpotential (η).

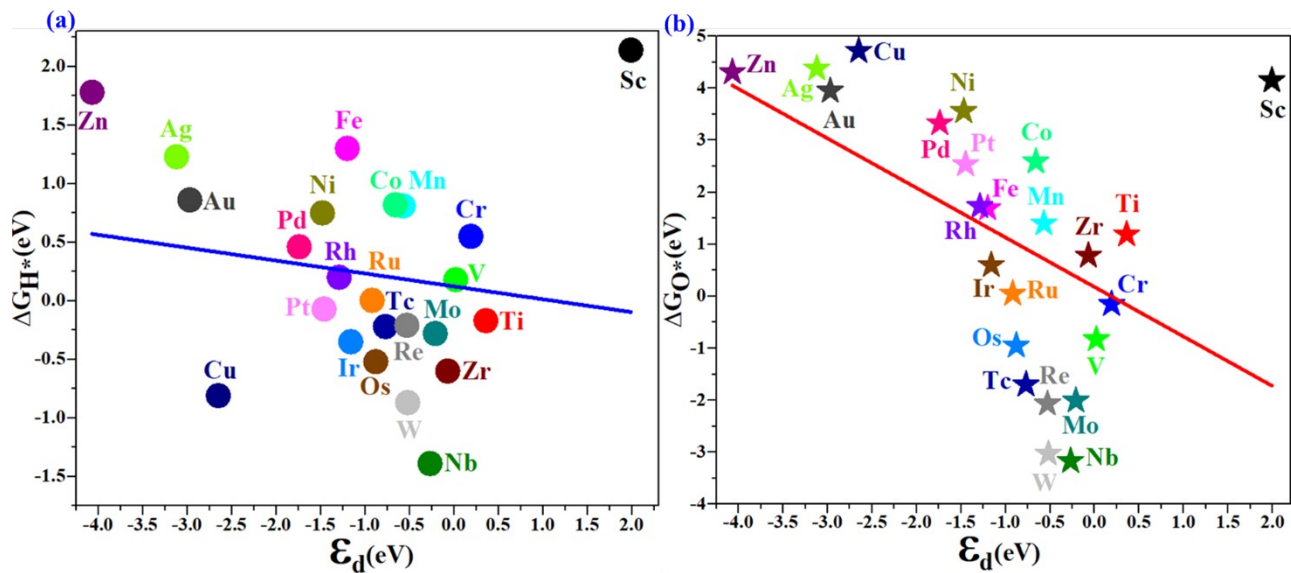**Fig. S19.** (a) Scaling relationship between the d-band centers and Gibbs free energy of adsorbed hydrogen atom (ΔG_{H*}) (b) Scaling relationship among the d-band centers of adsorbed transition metal and ΔG_{O*} intermediates for the M_1/PTA catalysts.

Table S2. The calculated total adsorption energy of H* intermediates (E_{H*}), Gibbs free energy of hydrogen adsorption (ΔG_{H*}), and d-band center of transition metal atoms over the surface of M_1/PTA (M_1 = Sc_1, Ti_1, V_1, Cr_1, Mn_1, Fe_1, Co_1, Ni_1, Cu_1, Zn_1, Zr_1, Nb_1, Mo_1, Tc_1, Ru_1, Rh_1, Pd_1, Ag_1, W_1, Re_1, Os_1, Ir_1, Pt_1, and Au_1,) catalysts. The unit for energy is eV.

Systems	E_{H*}	ΔG_{H*}	ε_d
Sc_1/PTA	-481.76517	2.14	1.99
Ti_1/PTA	-483.70976	-0.17	0.36
V_1/PTA	-483.07164	0.181	0.02
Cr_1/PTA	-482.61658	0.55	0.19
Mn_1/PTA	-481.87768	0.81	-0.57
Fe_1/PTA	-479.31548	1.30	-1.20
Co_1/PTA	-477.93277	0.82	-0.66
Ni_1/PTA	-476.08253	0.75	-1.48
Cu_1/PTA	-475.43861	-0.81	-2.65
Zn_1/PTA	-470.78417	1.78	-4.07
Zr_1/PTA	-484.97416	-0.60	-0.07
Nb_1/PTA	-484.4743	-1.39	-0.27
Mo_1/PTA	-482.87575	-0.28	-0.21
Tc_1/PTA	-480.86017	-0.22	-0.77
Ru_1/PTA	-479.02016	0.004	-0.92
Rh_1/PTA	-476.86409	0.20	-1.29
Pd_1/PTA	-474.2702	0.46	-1.74
Ag_1/PTA	-470.48831	1.23	-3.12
W_1/PTA	-484.62251	-0.87	-0.52
Re_1/PTA	-482.49357	-0.21	-0.53
Os_1/PTA	-480.3419	-0.52	-0.88
Ir_1/PTA	-477.99489	-0.35	-1.16
Pt_1/PTA	-475.29499	-0.08	-1.46
Au_1/PTA	-471.16318	0.86	-2.97

Table S3. The calculated adsorption energy of reaction intermediates (E_{OH*}, E_{O*}, E_{OOH*}) at the 4H site over M_1/PTA (M_1 = Sc_1, Ti_1, V_1, Cr_1, Mn_1, Fe_1, Co_1, Ni_1, Cu_1, Zn_1, Zr_1, Nb_1, Mo_1, Tc_1, Ru_1, Rh_1, Pd_1, Ag_1, W_1, Re_1, Os_1, Ir_1, Pt_1, and Au_1,) catalysts. The unit for energy is eV.

Systems	E_{OH*}	E_{O*}	E_{OOH*}
Sc_1/PTA	-490.35588	-483.70829	-494.87952
Ti_1/PTA	-492.729	-486.17378	-496.56709
V_1/PTA	-492.08923	-487.95165	-496.18375
Cr_1/PTA	-490.68065	-487.19302	-495.33524
Mn_1/PTA	-489.54795	-485.17938	-493.42825
Fe_1/PTA	-487.19929	-482.78759	-491.73249
Co_1/PTA	-485.11145	-480.03665	-489.63737
Ni_1/PTA	-482.72394	-477.10468	-487.36846
Cu_1/PTA	-479.43587	-473.57956	-484.50508
Zn_1/PTA	-478.31714	-472.12123	-482.94735
Zr_1/PTA	-494.16442	-487.42093	-498.35973
Nb_1/PTA	-493.59162	-490.10639	-497.66666
Mo_1/PTA	-491.48022	-488.48045	-496.29198
Tc_1/PTA	-498.27524	-486.22012	-493.99407
Ru_1/PTA	-486.8929	-482.83101	-491.52801
Rh_1/PTA	-484.11494	-479.25087	-488.45811
Pd_1/PTA	-480.75502	-475.20716	-485.34550
Ag_1/PTA	-477.20781	-471.09316	-483.44883
W_1/PTA	-493.49747	-490.63177	-498.47049
Re_1/PTA	-491.13786	-488.25458	-496.05693
Os_1/PTA	-488.17133	-484.60554	-493.00932
Ir_1/PTA	-485.02068	-480.93627	-489.56164
Pt_1/PTA	-481.57366	-476.47658	-486.00867
Au_1/PTA	-477.64712	-471.84598	-481.82915

Table S4. Binding energy (E), zero-point energy (ZPE), and entropic correction (TS, T = 298.15K) of the reactants and products. The unit for energy is eV.

Species	E	ZPE	TS
O_2	-9.860	0.1057	0.6300
H_2O	-14.216	0.5873	0.6700
H_2	-6.770	0.2719	0.4000

Table S5. The zero-point energy (ZPE) of the intermediates adsorbed over M_1/PTA (M_1 = Sc_1, Ti_1, V_1, Cr_1, Mn_1, Fe_1, Co_1, Ni_1, Cu_1, Zn_1, Zr_1, Nb_1, Mo_1, Tc_1, Ru_1, Rh_1, Pd_1, Ag_1, W_1, Re_1, Os_1, Ir_1, Pt_1, and Au_1,) catalysts. Notably, the ZPE of substrates is negligible, and the entropies of adsorbate and substrate are negligible as well.

| Systems	H*	*OH	*O	*OOH
Sc_1/PTA	0.028795	0.320496	0.030974	0.416476
Ti_1/PTA	0.170774	0.312390	0.051672	0.421849
V_1/PTA	0.173847	0.314059	0.082721	0.467119
Cr_1/PTA	0.171247	0.359294	0.085284	0.423191
Mn_1/PTA	0.160211	0.342266	0.084502	0.420497
Fe_1/PTA	0.175332	0.364781	0.078649	0.427974
Co_1/PTA	0.163899	0.320798	0.069990	0.441757
Ni_1/PTA	0.171921	0.349254	0.053537	0.435058
Cu_1/PTA	0.167213	0.337195	0.047307	0.418297
Zn_1/PTA	0.116921	0.325993	0.036501	0.432259
Zr_1/PTA	0.163989	0.319086	0.048109	0.456893
Nb_1/PTA	0.185307	0.327288	0.078428	0.441252
Mo_1/PTA	0.171811	0.339330	0.081187	0.319674
Tc_1/PTA	0.164624	0.356655	0.084360	0.333389
Ru_1/PTA	0.173045	0.377771	0.078268	0.430418
Rh_1/PTA	0.154813	0.361882	0.079217	0.438795
Pd_1/PTA	0.201153	0.352712	0.059438	0.415964
Ag_1/PTA	0.192300	0.334978	0.037266	0.385706
W_1/PTA	0.195933	0.320286	0.082762	0.333218
Re_1/PTA	0.161848	0.375864	0.089580	0.340221
Os_1/PTA	0.182917	0.380956	0.077183	0.401560
Ir_1/PTA	0.144938	0.376061	0.084485	0.428110
Pt_1/PTA	0.218376	0.363328	0.069474	0.449651
Au_1/PTA	0.226586	0.352979	0.056278	0.404807
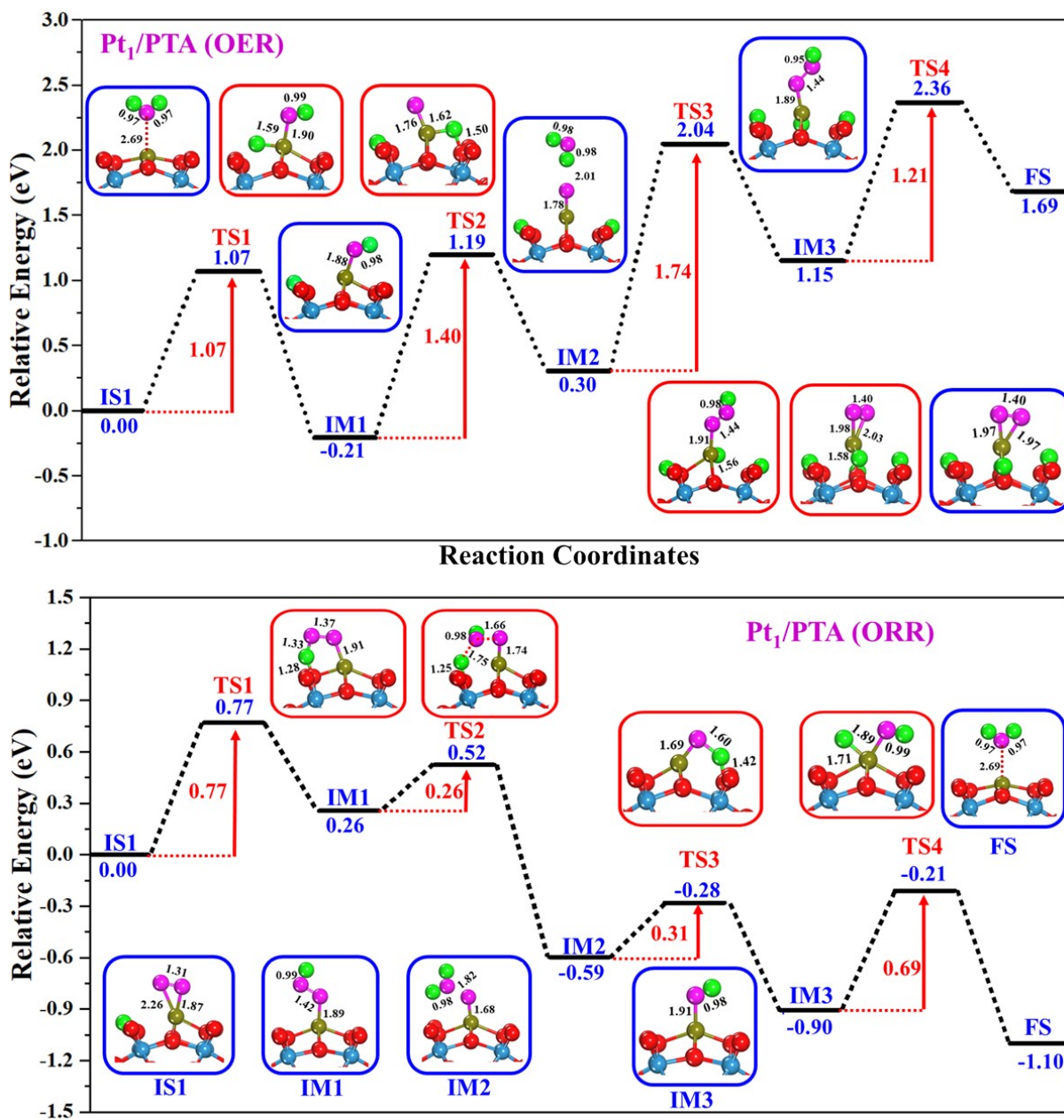
Fig. S20. The potential energy profile of the four successive elementary steps involved in the OER and ORR on the surface of Pt$_1$/PTA, respectively. All the energies are measured in eV.
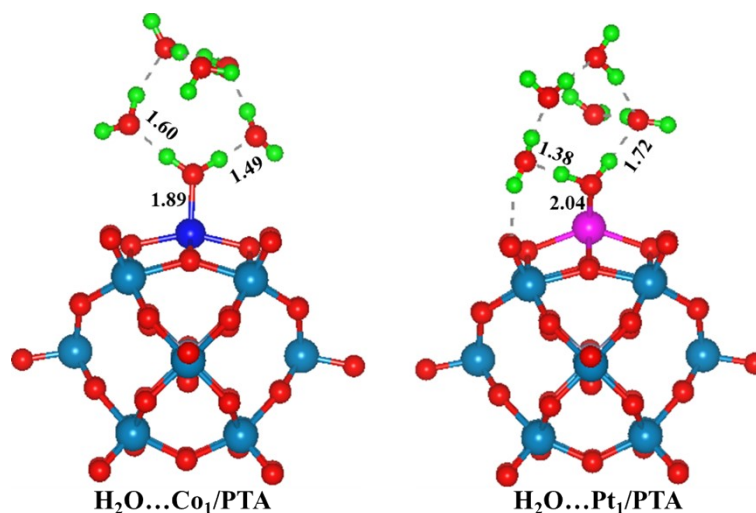
Fig. S21. Side views of a chemisorbed H_2O stabilized by H_2O molecules. The cobalt, platinum, tungsten, hydrogen, and oxygen atoms are denoted as blue, pink, sky-blue, green, and red spheres, respectively.
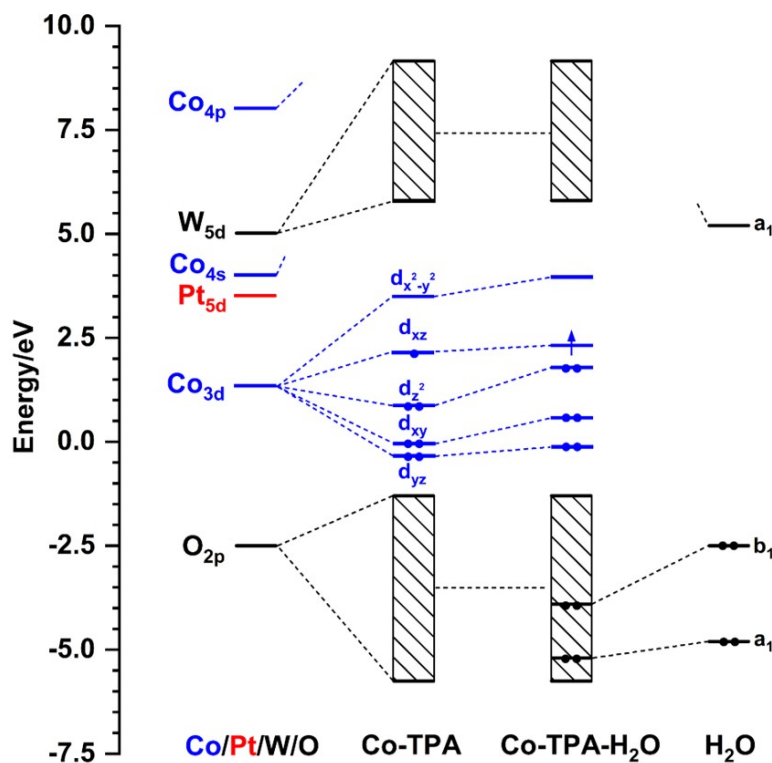

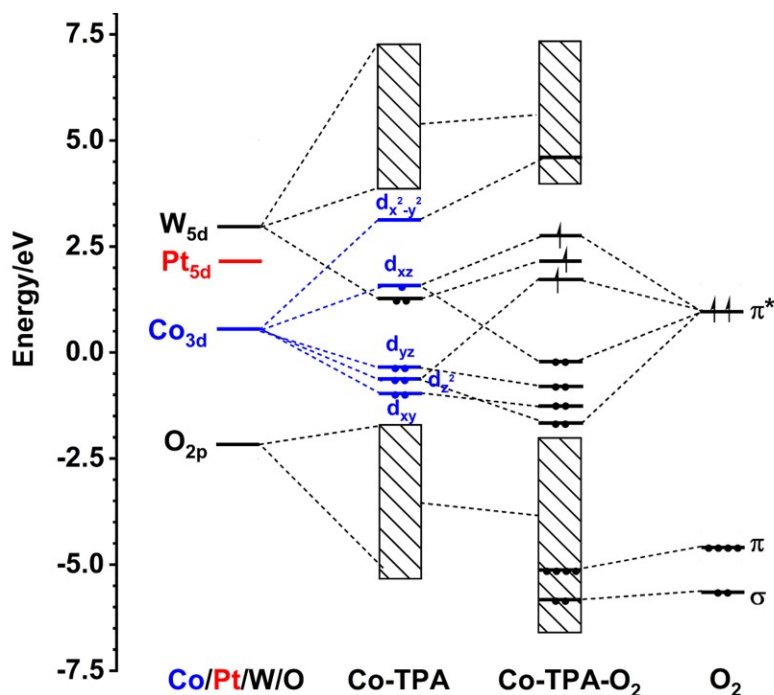**Fig. S22.** Kohn-Sham energy level of $Co_1/PTA-H_2O$ complexes with the fragments of C/PTA and H_2O molecules.

Fig. S23. Kohn-Sham energy level of Co_1/PTA-O_2 complexes with the fragments of Co_1/PTA and O_2 molecules. The calculations were performed with the ADF-2019.304 program at the hybrid PBE0 level. The uncontracted Slater-type basis sets with the quality of triple-ζ plus one polarization functions (TZP) were applied for Co/Pt/W atoms and the uncontracted Slater-type basis sets with the quality of double-ζ plus one polarization functions (DZP) were used for O atoms.

References

(1) Kresse, G.; Furthmüller, J. Efficiency of Ab-Initio Total Energy Calculations for Metals and Semiconductors using a Plane-Wave Basis Set. *Comput. Mater. Sci.* **1996,** *6*, 15-50.

(2) Kresse, G.; Furthmüller, J. Efficient Iterative Schemes for Ab Initio Total-Energy Calculations using a Plane-Wave Basis Set. *Phys. Rev. B.* **1996,** *54*, 11169-11186.

(3) Gajdoš, M.; Hummer, K.; Kresse, G.; Furthmüller, J.; Bechstedt, F. Linear Optical Properties in the Projector-Augmented Wave Methodology. *Phys. Rev. B.* **2006,** *73* 045112.

(4) Axel, D. Becke. Density-Functional Thermochemistry. III. The Role of Exact Exchange. *J. Chem. Phys.* **1993,** *98*, 5648-5652.

(5) Perdew, J. P.; Chevary, J. A.; Vosko, S. H.; Jackson, K. A.; Pederson, M. R.; Singh, D. J.; Fiolhais, C. Atoms, Molecules, Solids, and Surfaces: Applications of the Generalized Gradient Approximation for Exchange and Correlation. *Phys. Rev. B.* **1992,** *46*, 6671-6687.

(6) Assessment of the Perdew–Burke–Ernzerhof Exchange-Correlation Functional. *J. Chem. Phys.* **1999,** *110*, 5029-5036.

(7) Sancho-Garcı́a, J. C.; Brédas, J. L.; Cornil, J. Assessment of the Reliability of the Perdew–Burke–Ernzerhof Functionals in the Determination of Torsional Potentials in π-Conjugated Molecules. *Chem. Phys. Lett.* **2003,** *377*, 63-68.

(8) Canto, G.; Salazar-Ehuan, I.; González-Sánchez, J.; Tapia, A.; Quijano, R.; Simonetti, S. Density Functional Theory Study of the Hydrogen Storage in a Vacancy Zone of an Iron-Nickel Cell. *Int. J. Hydrogen Energ.* **2014,** *39*, 8744-8748.

(9) Lu, X.; T Morelli, D.; Xia, Y.; Ozolins, V. Supplementary Information to "Increasing the Thermoelectric Figure of Merit of Tetrahedrites by Co-doping with Nickel and Zinc*". Chem Mater* **2015**, *27*, 408–413.

(10) Zhao, S.; Liu, X.-W.; Huo, C.-F.; Li, Y.-W.; Wang, J.; Jiao, H. Determining Surface Structure and Stability of ε-Fe_2C, χ-Fe_5C_2, θ-Fe_3C and Fe_4C Phases under Carburization Environment from Combined DFT and Atomistic Thermodynamic Studies. *Catal.Struct. & Reactivity* **2015,** *1*, 44-60.

(11) Rossmeisl, J.; Qu, Z. W.; Zhu, H.; Kroes, G. J.; Nørskov, J. K. Electrolysis of Water on Oxide Surfaces *J. Electroanal. Chem.* **2007,** *607*, 83-89.

(12) Gao, G.; Waclawik, E. R.; Du, A. Computational Screening of Two-Dimensional Coordination Polymers as Efficient Catalysts for Oxygen Evolution and Reduction Reaction. *J. Catal.* **2017,** *352*, 579-585.

(13) Nørskov, J. K.; Rossmeisl, J.; Logadottir, A.; Lindqvist, L.; Kitchin, J. R.; Bligaard, T.; Jónsson, H. Origin of the Overpotential for Oxygen Reduction at a Fuel-Cell Cathode. *J. Phys. Chem. B* **2004,** *108*, 17886-17892.